Obliquely propagating dust-density waves

A. Piel,* O. Arp, and M. Klindworth
IEAP, Christian-Albrechts-Universität, D-24098 Kiel, Germany

A. Melzer
IfP, Ernst-Moritz-Arndt-Universität, Greifswald, Germany

(Received 10 October 2007; published 19 February 2008)

Self-excited dust-density waves are experimentally studied in a dusty plasma under microgravity. Two types of waves are observed: a mode inside the dust volume propagating in the direction of the ion flow and another mode propagating obliquely at the boundary between the dusty plasma and the space charge sheath. The dominance of oblique modes can be described in the frame of a fluid model. It is shown that the results fom the fluid model agree remarkably well with a kinetic electrostatic model of Rosenberg [J. Vac. Sci. Technol. A **14**, 631 (1996)]. In the experiment, the instability is quenched by increasing the gas pressure or decreasing the dust density. The critical pressure and dust density are well described by the models.

DOI: 10.1103/PhysRevE.77.026407 PACS number(s): 52.27.Lw, 52.27.Gr, 52.35.Fp, 82.70.Dd

I. INTRODUCTION

The dust acoustic wave (DAW) [1] is the archetype of a density wave in dusty plasmas in the low-frequency regime. This wave was predicted to become unstable in the presence of streaming ions (see, e.g., Refs. [2,3]) and unstable DAWs were observed in several experiments [4–18]. The DAW is mostly considered as a one-dimensional problem with the propagation direction aligned with the ion flow. Recently, dust density waves, which propagate at an oblique angle with respect to the ion streaming direction, were observed under microgravity conditions [19,20]. The phenomenon was discussed in terms of a simple fluid model, which predicted that a wide angular spectrum of waves can be excited and that the fastest growing mode undergoes a transition from propagation aligned with the ion flow at low ion velocity to oblique propagation when the drift approaches the Bohm velocity.

Observations of oblique wave modes in unmagnetized laboratory plasmas with an ion beam are rare. Buneman-type instabilities were found to have, under certain conditions, the fastest growing modes at an oblique angle with respect to the beam [21]. These modes were considered to be responsible for the excitation of a three-dimensional turbulence spectrum. On the other hand, the theory of oblique modes excited by relativistic electron beams for the fast ignitor concept was recently found rapidly expanding (e.g., Ref. [22,23]).

In the present article we investigate the oblique dust density modes in more detail. For this purpose calculations are made with our simple fluid model over an extended range of conditions. We compare the results with an earlier electrostatic kinetic model [24] that allows for including a finite temperature of the ion beam. In particular, we study the angular distribution of unstable modes as a function of beam velocity and determine the quenching of the instability as a function of gas pressure and dust density.

II. EXPERIMENTAL SETUP AND OBSERVATIONS

The experiments were performed in a 13.56 MHz radio-frequency (r.f.) parallel plate discharge under microgravity during the 6th and 7th DLR (German Aerospace Center) parabolic flight campaign (2005). The construction of the original IMPF (International Microgravity Plasma Facility) device was described in Ref. [25].

A vertical cross section through the center of the presently used modified IMPF-K (K="Kiel") device is shown in Fig. 1. The electrodes are segmented and consist of a central disk and two concentric rings. The r.f. discharge is operated with two independent r.f. power generators. The first feeds the upper and lower disk electrodes in a push-pull mode. The ring electrodes are pairwise connected and powered by the second generator. The axial gap between the electrodes is 30 mm wide and the outer ring has a diameter of 80 mm. The IMPF-K device is equipped with the two-dimensionally scanning Langmuir probe system for measuring the plasma parameters described in Ref. [25].

The r.f. discharge is operated in argon at pressures of (15–50) Pa. Typical r.f. voltages are $U_{\mathrm{rf}}=(50-100)\ V_{pp}$. We use monodisperse melamine particles of radius $a=3.4\ \mu$m. Typical plasma conditions are ion density $n_i \approx 1\times 10^{15}\ \mathrm{m}^{-3}$ and electron temperature $T_e=(2.5-4)$ eV. A detailed investigation of plasma parameters in the IMPF-K device was presented in Ref. [26]. This device is also used for laser manipulation of dust particles [27,28].

DDWs are observed with a vertically expanded sheet of laser light and a fast digital video camera. The useable field

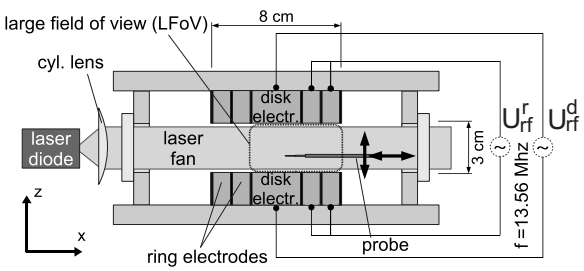

FIG. 1. Side view of the IMPF-K device. The r.f. discharge has segmented electrodes and is operated in push-pull mode between pairs of electrodes. The two ring electrodes are electrically connected.

*piel@physik.uni-kiel.de

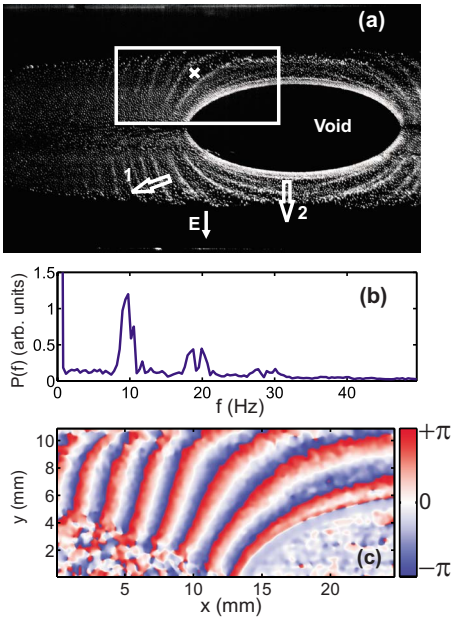

FIG. 2. (Color online) (a) Still image of the dust-density wave. The arrows indicate the different wave propagation directions in regions 1 and 2. The electric field direction is perpendicular to the sheath boundary. (b) Spectral power density $P(f)$ of the dust density wave. (c) Reconstructed phase fronts of the dust density wave.

of view is 60×30 mm^2 as indicated in Fig. 1. The camera is positioned at the rear window of the chamber, which results in an image in which left and right are interchanged. The corresponding camera resolution is 1280×640 pixels. The frame rate was chosen as 100 fps to avoid any aliasing of wave signals, which have frequencies of $f\approx10$ Hz.

Self-excited DDWs are found at low gas pressure and high dust density. The following results were obtained at the standard conditions $p=15$ Pa and $U_{\mathrm{rf}}^{d}=65$ V_{pp}. Inner and outer ring were operated at $U_{\mathrm{rf}}^{r}=55$ V_{pp}. A typical still image, which represents a central vertical section through the dust cloud, is shown in Fig. 2(a). The dust distribution shows the formation of a central dust-free region ("void"), an oval ring of dust and a dark dust-free space-charge sheath in front of both electrodes. The boundary of the dust cloud is identified with the edge of the space-charge sheath. The formation of the central void was seen in many similar investigations, e.g., in Refs. [29–31]. The void mechanism is explained by a force balance between the ion-drag force from the ambipolar ion-flow out of the plasma center and the ambipolar electric field force [32].

The waves are seen as a strong spatial modulation of the dust density. Close to the void edge, the wave fronts (visible as bright wave crests) move vertically away from the void (arrow 2) with a velocity of $v_{\mathrm{DDW}}\approx20$ mm s^{-1}. Farther away from the void, the wave fronts change their orientation and finally become strongly inclined with respect to the sheath edge (arrow 1). A similar pattern is found in the upper part of the dust cloud. These two regions are separated by a stripe of reduced wave activity in the midplane between the electrodes.

The dramatic change in wave propagation direction was not expected for the ordinary DAW, because the ion flow that excites the unstable DDW is aligned with the static electric field. Since this electric field is also responsible for the force equilibrium of the dust particles at the edge of the dust cloud, the electric field must be strictly perpendicular to the dust boundary. Otherwise, a dust flow along the boundary would be observed. Simulations of a dusty plasma in a smaller device [33] show that the radial ambipolar field is much smaller than the field at the sheath boundary. Because our device has a two times larger electrode diameter but a comparable gap width, we consider the influence of a radial field or edge effects of the electrodes as negligible. We call this unusual wave type an "obliquely propagating dust-density wave" (OPDDW).

The frequency of the OPDDW is determined at the marked position in Fig. 2(a) from the spectral power density shown in Fig. 2(b), $f_{\mathrm{OP}}=9.5$ Hz, and the propagation velocity, as obtained from the displacement of the wave fronts in subsequent frames, is $v_{\mathrm{OP}}\approx20$ mm s^{-1}. This propagation velocity is similar to v_{DDW} found at the void edge.

The time averaged phase fronts of the OPDDW can be visualized in more detail by a Fourier analysis of the brightness of each pixel $B(x,y,t)$. The complex wave function $C(x,y)+iS(x,y)$ corresponding to f_{OP} is calculated as

$$C(x,y)=\sum_{i=1}^{N}B(x,y,t_i)\cos(2\pi f_{\mathrm{OP}}t_i), \tag{1}$$

$$S(x,y)=\sum_{i=1}^{N}B(x,y,t_i)\sin(2\pi f_{\mathrm{OP}}t_i). \tag{2}$$

The phase distribution is then $\phi(x,y)=\arctan[S(x,y)/C(x,y)]$. The result is shown in Fig. 2(c). The wave fronts are found to have an inclination of $\theta=(40-80)°$ with respect to the sheath boundary. The mean wavelength is $\lambda=(2\pm0.5)$ mm. Self-excited waves are only observed at high dust density and below a critical gas pressure $p_{\mathrm{crit}}\approx40$ Pa. The nearly equal propagation speeds of the wave in the two regimes means that the wavelength remains practically the same.

III. FLUID MODEL FOR THE OPDDW

The DDW is described by the electrostatic dispersion relation [2]

$$0=1+\chi_e+\chi_i+\chi_d, \tag{3}$$

which contains the susceptibilities of the electrons, ions, and dust particles. In a fluid description the electron susceptibility has the form [3]

$$\chi_e=-\frac{\omega_{pe}^2}{\omega(\omega+i\nu_e)-\gamma_e k^2 v_{Te}^2}. \tag{4}$$

Because the wave frequency ω is very small compared to the electron plasma frequency ω_{pe}, the electrons are isothermal ($\gamma_e=1$). Neglecting electron-neutral collisions the electron response is adequately represented by $\chi_e=(k\lambda_{De})^{-2}$. Here, k is the wave number, $\lambda_{De}=v_{Te}/\omega_{pe}=[\epsilon_0 k_B T_e/(n_e e^2)]^{1/2}$ the

electron Debye length, $v_{Te}=(k_BT_e/m_e)^{1/2}$ the electron thermal velocity.

The susceptibility of the dust

$$\chi_d = -\frac{\omega_{pd}^2}{\omega(\omega+i\nu_{dn})-\gamma_d k^2 v_{Td}^2} \tag{5}$$

depends on the dust plasma frequency $\omega_{pd}=[Z_d^2e^2n_d/(\epsilon_0 m_d)]^{1/2}$ (Z_d, n_d, m_d being the dust charge number, density, and mass), the wave frequency ω and the dust-neutral collision frequency ν_{dn}. The kinetic pressure of the dust is included in terms of the dust thermal velocity $v_{Td}=(k_BT_d/m_d)^{1/2}$. The dust compression is considered adiabatic with $\gamma_d=3$.

The ion susceptibility is derived from a fluid model that includes a streaming velocity v_{i0} in z direction, a thermal velocity $v_{Ti}=(k_BT_i/m_i)^{1/2}$ and a collision frequency ν_i, which accounts for ion collisions with neutral atoms and dust particles. Note, that the original version of the fluid model [19] contained an error, which was corrected in the Erratum [20].

The calculation starts from the linearized equation of motion for the ions in the electric field of a plane wave $\phi(\vec{r},t)=\tilde{\phi}\exp[i(\vec{k}\cdot\vec{r}-\omega t)]$

$$\frac{\partial v_{ix}}{\partial t}+v_{i0}\frac{\partial v_{ix}}{\partial z}+\nu_i v_{ix}=-\frac{e}{m_i}\frac{\partial\phi}{\partial x}-\frac{\gamma_i v_{Ti}^2}{n_{i0}}\frac{\partial n_i}{\partial x}, \tag{6}$$

$$\frac{\partial v_{iz}}{\partial t}+v_{i0}\frac{\partial v_{iz}}{\partial z}+\nu_i v_{iz}=-\frac{e}{m_i}\frac{\partial\phi}{\partial z}-\frac{\gamma_i v_{Ti}^2}{n_{i0}}\frac{\partial n_i}{\partial z}, \tag{7}$$

and the linearized equation of continuity

$$\frac{\partial n_i}{\partial t}+v_{i0}\frac{\partial n_i}{\partial x}+n_{i0}\left(\frac{\partial v_{ix}}{\partial x}+\frac{\partial v_{iz}}{\partial z}\right)=0. \tag{8}$$

Assuming the same wave dependence $\propto\exp[i(\vec{k}\cdot\vec{r}-\omega t)]$ for the fluctuating quantities n_i, v_{ix}, and v_{iz}, the equations of motion and continuity take the form

$$-i\Omega_1\tilde{v}_{ix}=-ik_x\frac{e}{m_i}\tilde{\phi}-ik_x\frac{v_{Ti}^2}{n_{i0}}\tilde{n}_i, \tag{9}$$

$$-i\Omega_1\tilde{v}_{iz}=-ik_z\frac{e}{m_i}\tilde{\phi}-ik_z\frac{v_{Ti}^2}{n_{i0}}\tilde{n}_i, \tag{10}$$

$$0=-\Omega_2\tilde{n}_i+(k_x\tilde{v}_{ix}+k_z\tilde{v}_{iz})n_{i0}. \tag{11}$$

Here, the response of the ions is determined by the Doppler shifted and collision modified frequency $\Omega_1=\omega-k_zv_0+i\nu_i$. The continuity equation involves the Doppler shift $\Omega_2=\omega-k_zv_0$. Finally, we obtain the ion susceptibility $\chi_i=-(e\tilde{n}_i)/(\epsilon_0k^2\tilde{\phi})$ as a function of the orientation angle $\theta=\arccos(k_z/k)$ between k and ion beam direction z

$$\chi_i=\frac{-\omega_{pi}^2}{\Omega_1\Omega_2-\gamma_i k^2 v_{Ti}^2}. \tag{12}$$

We note here that in the collisionless limit the fluid susceptibility has a singularity at $\Omega_1^2=\gamma_i k^2 v_{Ti}^2$, which is not present in the kinetic theory.

Equation (12) gives the well-known limiting cases, (a) for stationary warm and collisionless ions $\chi_i\approx(k\lambda_{Di})^{-2}$ with the ion Debye length $\lambda_{Di}=v_{Ti}/\omega_{pi}$ and (b) for stationary cold ions: $\chi_i\approx-\omega_{pd}^2/\omega(\omega+i\nu_i)$. Since, in χ_i, the wave frequency ω can be neglected compared to the ion collision frequency, the dispersion relation Eq. (3) can be solved explicitly for a complex ω

$$\omega=-\frac{i}{2}\nu_{dn}+\left(-\frac{1}{4}\nu_{dn}^2+\frac{\omega_{pd}^2}{1+\chi_e+\chi_i}\right)^{1/2}. \tag{13}$$

The positive root was chosen as it gives the correct limiting case of an ordinary DAW when $\nu_{dn}\to0$.

IV. KINETIC MODEL FOR OBLIQUE MODES

For comparison with the fluid model of the OPDDW we now consider the kinetic electrostatic model used by Rosenberg [24] to study the properties of oblique dust density waves. The following expression for the susceptibilities is used [34,35]:

$$\chi_\alpha=\frac{1}{k^2\lambda_{D\alpha}^2}\frac{1+\zeta_\alpha Z(\zeta_\alpha)}{1+(i\nu_\alpha/\sqrt{2}kv_{T\alpha})Z(\zeta_\alpha)} \tag{14}$$

with $\alpha=d,i,e$, and

$$\zeta_i=\frac{\omega-k_zv_{i0}+i\nu_i}{\sqrt{2}kv_{Ti}},\quad \zeta_{e,d}=\frac{\omega+i\nu_{e,d}}{\sqrt{2}kv_{Te,Td}}, \tag{15}$$

where $\lambda_{D\alpha}=[\epsilon_0k_BT_\alpha/(n_{\alpha0}Z_\alpha^2e^2)]^{1/2}$ is the Debye length of species α and $Z(\zeta)$ the plasma dispersion function [36].

For practical calculations we first inspect the necessity of treating the electrons by the kinetic model. The wave frequency ω is of the order of the dust plasma frequency ω_{pd}, which is usually six orders of magnitude smaller than ω_{pe}. On the other hand, the electron-neutral collision frequency is typically in the range $\nu_e\approx(0.01-0.3)\omega_{pe}$. Hence we can neglect ω compared to $i\nu_e$ in the definition of ζ_e. In this limit, the electron susceptibility reduces exactly to $\chi_e=(k\lambda_{De})^{-2}$. Although the electrons are weakly collisional, their effect on the low-frequency wave is only a shielding action. The physical interpretation is that, despite the friction, the electrons are always able to attain their equilibrium positions in the wave potential because the wave frequency is so low. Hence, we do not expect wave damping by electron friction.

For the dust component, we argue that $|\zeta_d|\gg1$. From our fluid results we expect that $\omega\simeq\omega_{pd}$ and $k\lambda_{De}\simeq1-5$. Therefore, the quantity ζ_d becomes

$$\zeta_d\approx\frac{1}{2\pi\sqrt{2}(k\lambda_{De})}\frac{\lambda_{De}}{\lambda_{Dd}}\left(1+i\frac{\nu_d}{\omega_{pd}}\right) \tag{16}$$

with $\lambda_{Dd}=v_{Td}/\omega_{pd}$. For our experimental conditions $\lambda_{De}/\lambda_{Dd}\simeq420$, $\nu_d/\omega_{pd}\simeq0.3$, which gives $|\zeta_d|\approx(9-50)$. Using the asymptotic expansion $Z(\zeta)\approx-\zeta^{-1}-(1/2)\zeta^{-3}-(3/4)\zeta^{-5}$ we obtain the fluidlike result

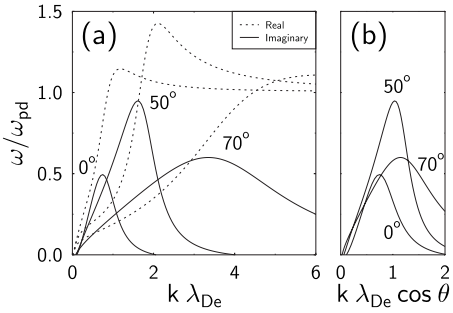

FIG. 3. (a) Unstable oblique modes at the conditions of Ref. [24]. (b) The maximum growth rate is found at $k\lambda_{De}\cos\theta \approx 1$.

$$\chi_d = \frac{-\omega_{pd}^2}{\omega(\omega + i\nu_d) - [3 - 2\nu_d/(\nu_d - i\omega)]k^2 v_{Td}^2}. \qquad (17)$$

Note that the fluid result Eq. (5) for adiabatic compression ($\gamma_d = 3$) is recovered in the limit $\nu_d \ll \omega$ whereas $\gamma = 1$ is approached for $\nu_d \gg \omega$. Since the thermal correction is small, $k^2 v_{Td}^2 \ll \omega^2$, we can neglect the collisional part of the thermal correction and use Eq. (5) for the dust susceptibility.

For the ion susceptibility now the full kinetic form of $Z(\zeta)$ is retained in order to demonstrate the differences from the fluid model. The fluid limit for χ_i [Eq. (12)] can be recovered, when an asymptotic expansion ($|\zeta_i| \gg 1$) is justified. However, this expansion is not valid at low drift velocity $v_{i0} \ll v_B \lesssim 10 v_{Ti}$ or large θ because, in the low-collision limit, $\zeta_i \approx 0.7 v_{i0}\cos(\theta)/v_{Ti}$ can be close to unity.

For the calculation of the plasma dispersion function the Padé approximation with eight poles [37,38] is used. Comparing samples in the upper half of the complex ζ plane with the tables in Ref. [36] we found agreement in six significant digits. Neglecting again the wave frequency ω in χ_i, the dispersion relation is solved in the form (13).

As a test of the validity of the entire approach, we have recalculated the example in Fig. 1 of Ref. [24], which refers to the typical situation at the sheath edge of a processing plasma with fine grains of 0.3 μm radius. The other parameters are $n_d/n_i = 3 \times 10^{-4}$, $Z_d = 1000$, $T_e/T_i = T_e/T_d = 40$, $m_d/m_p = 10^{11}$, $m_i/m_p = 40$, $\nu_e/\omega_{pe} = 0.3$, $\nu_i/\omega_{pe} = 10^{-3}$, $\nu_d/\omega_{pd} = 10^{-7}$. We find agreement with Ref. [24] within the graphical resolution. For convenience, the resulting growth rate and wave dispersion are shown in Fig. 3(a). The graph (a) shows the normalized wave frequency ω/ω_{pd} and growth rate γ/ω_{pd} as a function of wave number for different propagation angles θ between wave vector and ion drift direction. Note that at the maximum growth rate the relation $\omega \approx \gamma$ holds. This is a typical feature of a dissipative instability. In panel (b) the same growth rate curves are plotted against $k\lambda_{De}\cos\theta$. The maximum growth rate is found close to $k\lambda_{De}\cos\theta \approx 1$. This is evidence for the resonance condition of the beam ions $\omega_{pi} = k\cos\theta v_{i0}$ and shows that the mechanism is similar to a Buneman instability [24].

V. COMPARISON OF THE MODELS

The results from the fluid and kinetic model are compared at the typical conditions of our experiment. The dust particles (melamine-formaldehyde; $\rho = 1500$ kg m^{-3}) have a radius of $a = 3.4$ μm and carry a charge $Z_d = 4000$. The dust number density is $n_d = 5 \times 10^{10}$ m^{-3}. Argon gas with a pressure of $p = 15$ Pa at room temperature ($k_B T_d = 0.025$ eV) is assumed. The ion density is fixed at $n_i = 1.0 \times 10^{15}$ m^{-3} and the electron density follows from the quasineutrality condition $n_e = n_i - Z_d n_d$. The ions are assumed cold, $T_i = T_d$ whereas the electron temperature is $k_B T_e = 2.5$ eV. The ion neutral collisions obey the relation $\nu_{in} = v_0/\lambda$ with $\lambda(m) = 3.28 \times 10^{-3}/p(\mathrm{Pa})$ [39]. Ion-dust collisions, which are less frequent at these conditions [40] are presently neglected.

In Fig. 4 the comparison is shown of the growth rates of the unstable waves (in units of ω_{pd}) from the fluid model (a)–(c) with the kinetic model (d)–(f). The velocity of the ion beam was varied from $0.3 v_B$ to $1.0 v_B$, where $v_B = (k_B T_e/m_i)^{1/2}$ is the Bohm velocity. The angle of wave propagation with respect to the ion beam is varied from 0° to 80°.

The comparison shows that the characteristic features reported in Refs. [19,20] are confirmed by the kinetic model. At the lowest ion beam velocity $v_{i0} = 0.3 v_B$, the preferred wave propagation in the kinetic model is aligned with the ion flow. The fluid model predicts a wider range of unstable oblique waves. For increasing beam velocity the wave propagation direction becomes oblique in both models and reaches 70° at $v_{i0} = 0.7 v_B$. A further increased beam velocity leads to a strong damping of all modes with $\theta < 40°$ and leaves the most unstable mode at larger angles $\geqslant 80°$. The growth rates of the fluid model and the kinetic model have generally similar values with the exception of low drift and large angles. The wave number of the most unstable mode is confirmed. Thus, both the fluid model and the kinetic model are suitable to describe the transition from field-aligned to oblique wave propagation. The agreement can be understood as reaching the asymptotic limit $|\zeta_i| \gg 1$, where the fluid model becomes a suitable approximation. The difference between fluid and kinetic model at low drift and large angles may be attributed to ion Landau damping. For the sake of accuracy we will use the full kinetic model in the further analysis.

A more detailed analysis of the instability is compiled in Fig. 5 as a function of ion beam velocity. In panel (a) it becomes evident that the propagation angle changes direction to oblique propagation as soon as $v_{i0} > 0.3 v_B$. The wavelength increases in the regime $v_i/v_B = 0.1$–0.3 but remains nearly constant for $v_{i0}/v_B = 0.3$–1.0. The weak variation of the wavelength is in accordance with the experimental observation of nearly constant propagation speed.

Panel (b) gives the same information in terms of the parallel and perpendicular wave number. The parallel wave number $k_z = k\cos\theta$ decreases monotonically in the entire ion velocity range. The dashed line represents a fit function $k_z\lambda_{De} \approx 0.8(v_{i0}/v_B)^{-1}$, which describes the decrease of the parallel wave number quite well. This is the expected tendency which originates from the coupling of the ion beam fluctuations to the dust density fluctuations $\omega_{pi} = k_z v_{i0}$, and noting that $v_B = \omega_{pi}\lambda_{De}$.

The perpendicular wave number k_x increases between $0.3 \leqslant v_{i0}/v_B \leqslant 0.6$ and remains nearly constant at higher velocities. Panel (c) shows that the (real) frequency of the most

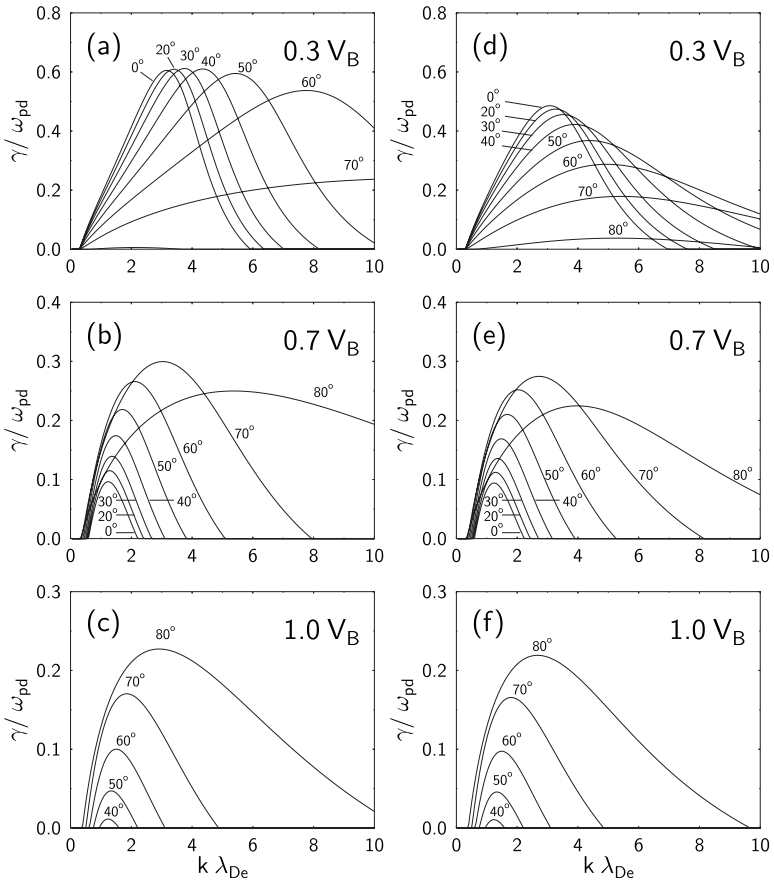

FIG. 4. Comparison of the growth rates predicted by the fluid model (a)–(c) and the kinetic model (d)–(f) for ion beam velocities of $0.3v_B$, $0.7v_B$, and $1.0v_B$. The other parameters are taken from our experiment. The curves are labeled with the propagation angle $\theta=0°-80°$.

unstable mode remains between $(0.6–0.8)\omega_{pd}$, whereas the growth rate attains a maximum $\gamma_{\max}\approx 0.5\omega_{pd}$ at $v_{i0}=0.3v_B$.

VI. QUENCHING OF THE INSTABILITY

In order to verify the quenching of the instability we have calculated the growth rates for different beam velocities using the kinetic model. The plasma parameters are the typical experimental values given above. In a first run the gas pressure was varied from (2–40) Pa (see Fig. 6). The growth rate is a monotonically decreasing function of gas pressure and the critical pressure for quenching lies in the range (35–45) Pa, which is in good agreement with the experimental observation. In a second run, we have reduced the dust density (Fig. 7). The critical dust density for quenching lies below $n_d=10^{10}$ m^{-3}, but is also dependent on beam velocity.

VII. DISCUSSION AND CONCLUSIONS

The appearance of unstable obliquely propagating modes has been observed in all our experiments under microgravity when the dust density exceeded a critical value and the gas pressure was ≈35 Pa or lower. OPDDWs are found close to the upper and lower sheath boundary of the discharge. These two regions are separated by a central stripe of reduced wave activity. Generally, we find that the dust density in the midplane is significantly reduced, as was also observed by other authors [41,42]. This observation suggests that wave excitation and propagation are determined by the local properties of the dust cloud. Moreover, the locality justifies the approach to explain the wave properties in terms of the local dispersion relation.

The experimental findings of OPDDWs have been compared with a fluid model and a kinetic model. The fluid model is found as the asymptotic limit of the full kinetic model [24]. Differences between the two models become visible when the drift velocity is low or the propagation angle becomes large. The comparison of both models shows that the appearance of OPDDWs is a robust phenomenon.

The presented analysis of the angular wave spectrum has shown that the limiting cases of parallel and oblique wave propagation can be well understood. For an ion drift speed of $v_{i0}\leqslant 0.3v_B$, which is a reasonable value inside the bulk of the dust cloud, the preferred wave propagation direction is $\theta=0°$. On the other hand, close to the sheath boundary, the ion drift velocity must approach the Bohm velocity. The assumption to identify the boundary of the dust cloud with the sheath edge is justified by our experience from dust clouds trapped close to a Langmuir probe [31], where the boundary of the dust cloud was found in the plasma region but very close to the sheath edge. According to the models, the maximum growth occurs for an oblique angle, which, however, depends on the actual local value of the ion drift velocity. This is in general accordance with the experimental observation of $\theta=(40°–80°)$. A more detailed comparison would indeed require a simulation of the electric field distribution with respect to magnitude and orientation inside the dust cloud.

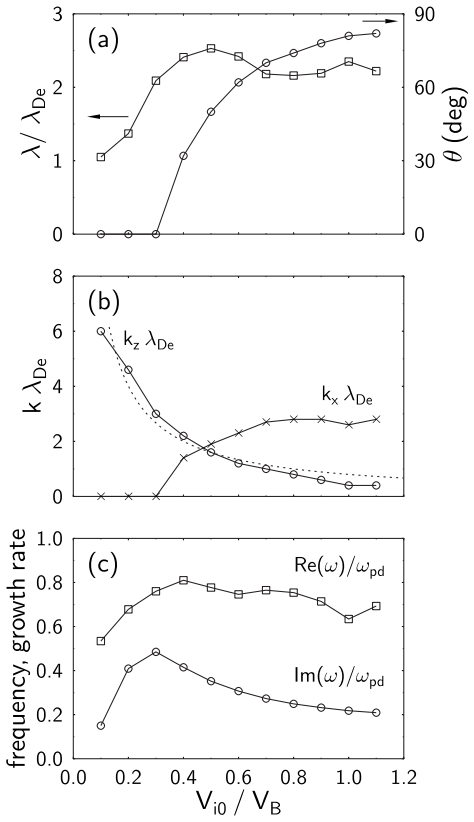

FIG. 5. Properties of the most unstable wave in the kinetic model as a function of the beam velocity. (a) Wavelength in units of the electron Debye length (squares) and propagation angle (circles). (b) Normalized perpendicular wavenumber $k_x\lambda_{De}$ and parallel wavenumber $k_z\lambda_{De}$. The dashed line is a fit $\propto v_{i0}^{-1}$. (c) Real frequency and growth rate in units of the dust plasma frequency.

Both models predict that the wavelength is only a weak function of the ion beam velocity for v_{i0}/v_B=0.3–1.0. This is consistent with the experimental observation of a practically constant propagation velocity of the field-aligned and oblique wave.

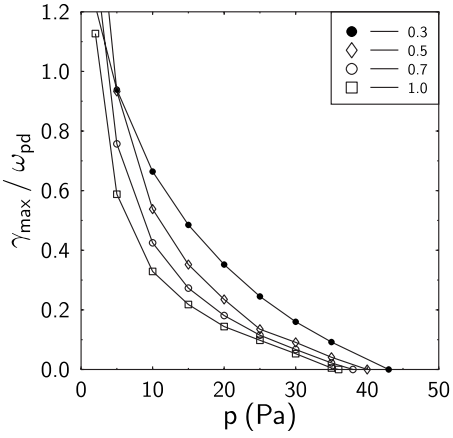

FIG. 6. Quenching of the instability by increasing the gas pressure. The different curves are labeled by the normalized ion beam velocity v_{i0}/v_B.

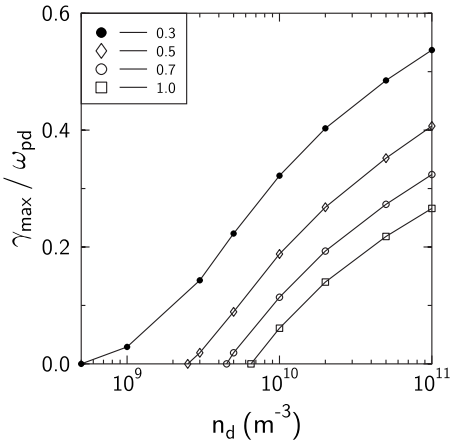

FIG. 7. Quenching of the instability by reducing the dust density. The different curves are labeled by the normalized ion beam velocity v_{i0}/v_B.

At the plasma parameters of our experiment, the present study has shown that both the fluid model and the kinetic model predict the preference for oblique wave propagation as soon as the ion beam velocity exceeds 30% of the Bohm velocity. The propagation angle of maximum growth rate as well as the corresponding wave number have very similar values in both models.

The quenching of the instability by increasing the pressure or lowering the dust density is confirmed by both models. The critical pressure is found only weakly dependent on the ion beam velocity. Its value is in close agreement with the experiment. The critical dust density, however, shows a stronger dependence on ion velocity. The quenching of field-aligned dust fluctuations in the vicinity of the sheath edge by ion and dust collisions with neutrals was reported before in Ref. [43]. Our model extends this discussion to oblique modes.

Future work on these oblique modes would benefit very much from detailed simulations similar to Ref. [44]. Although those simulations were performed for the PKE experiments under microgravity, which is smaller than IMPF-K, two of our assumptions are generally confirmed. First, in the region between the electrodes, the outer contour of the dust cloud is found to match the contours of constant ion velocity. Since the ion velocity is friction limited, the velocity contours are also equipontials. Hence, the electric field at the dust boundary is perpendicular to the dust boundary as stated above. Second, the ion velocity rises from typically $3v_{Ti}$ inside the dust cloud to (5–6) v_{Ti} at the outer dust boundary. This corresponds to a transition from roughly $0.2v_B$ to $(0.4–0.5)v_B$. A change from parallel to oblique propagation can therefore be expected from this simulation.

ACKNOWLEDGMENTS

This work was supported by DLR under Contracts Nos. 50WM0338 and 50WM0339, and in parts by Grant No. DFG-TR24/A2. The expert technical assistance by M. Poser and V. Rohwer is gratefully acknowledged.

[1] N. N. Rao, P. K. Shukla, and M. Y. Yu, Planet. Space Sci. **38**, 543 (1990).
[2] P. K. Shukla and M. M. Mamun, *Introduction to Dusty Plasma Physics* (IOP, Bristol, 2002).
[3] F. Verheest, *Waves in Dusty Space Plasmas* (Kluwer Academic, Dordrecht, 2000).
[4] A. Barkan, R. L. Merlino, and N. D'Angelo, Phys. Plasmas **2**, 3563 (1995).
[5] C. Thompson, A. Barkan, N. D'Angelo, and R. L. Merlino, Phys. Plasmas **4**, 2331 (1997).
[6] V. I. Molotkov, A. P. Nefedov, V. M. Torchinskii, V. E. Fortov, and A. G. Khrapak, JETP **89**, 477 (1999).
[7] V. E. Fortov, A. G. Khrapak, S. A. Khrapak, V. I. Molotkov, A. P. Nefedov, O. F. Petrov, and V. M. Torchinsky, Phys. Plasmas **7**, 1374 (2000).
[8] E. Thomas, Phys. Plasmas **8**, 329 (2001).
[9] A. V. Zobnin, A. D. Usachev, O. F. Petrov, and V. E. Fortov, JETP **95**, 429 (2002).
[10] V. E. Fortov, A. D. Usachev, A. V. Zobnin, V. I. Molotkov, and O. F. Petrov, Phys. Plasmas **10**, 1199 (2003).
[11] S. Khrapak *et al.*, Phys. Plasmas **10**, 1 (2003).
[12] S. Ratynskaia, M. Kretschmer, S. Khrapak, R. A. Quinn, M. H. Thoma, G. E. Morfill, A. Zobnin, A. Usachev, O. Petrov, and V. Fortov, IEEE Trans. Plasma Sci. **32**, 613 (2004).
[13] S. Ratynskaia *et al.*, Phys. Rev. Lett. **93**, 085001 (2004).
[14] T. Trottenberg, D. Block, and A. Piel, Phys. Plasmas **13**, 042105 (2006).
[15] E. Thomas, Jr., Phys. Plasmas **13**, 042107 (2006).
[16] E. Thomas, Jr., R. Fisher, and R. L. Merlino, Phys. Plasmas **14**, 123701 (2007).
[17] I. Pilch, A. Piel, T. Trottenberg, and M. E. Koepke, Phys. Plasmas **14**, 123704 (2007).
[18] M. Schwabe, M. Rubin-Zuzic, S. Zhdanov, H. M. Thomas, and G. E. Morfill, Phys. Rev. Lett. **99**, 095002 (2007).
[19] A. Piel, M. Klindworth, O. Arp, A. Melzer, and M. Wolter, Phys. Rev. Lett. **97**, 205009 (2006).
[20] A. Piel, M. Klindworth, O. Arp, A. Melzer, and M. Wolter, Phys. Rev. Lett. **99**, 209903(E) (2007).
[21] T. D. Mantei, F. Doveil, and D. Gresillon, Plasma Phys. **18**, 705 (1976).
[22] A. Bret, M.-C. Firpo, and C. Deutsch, Phys. Rev. E **70**, 046401 (2004).
[23] A. Bret, M.-C. Firpo, and C. Deutsch, Phys. Rev. E **72**, 016403 (2005).
[24] M. Rosenberg, J. Vac. Sci. Technol. A **14**, 631 (1996).
[25] M. Klindworth, O. Arp, and A. Piel, J. Phys. D **39**, 1095 (2006).
[26] M. Klindworth, O. Arp, and A. Piel, Rev. Sci. Instrum. **78**, 033502 (2007).
[27] M. Wolter, A. Melzer, O. Arp, M. Klindworth, and A. Piel, IEEE Trans. Plasma Sci. **35**, 266 (2007).
[28] M. Wolter, A. Melzer, O. Arp, M. Klindworth, and A. Piel, Phys. Plasmas **14**, 123707 (2007).
[29] G. Praburam and J. Goree, Plasma Sources Sci. Technol. **5**, 84 (1996).
[30] G. E. Morfill, H. M. Thomas, U. Konopka, H. Rothermel, M. Zuzic, A. Ivlev, and J. Goree, Phys. Rev. Lett. **83**, 1598 (1999).
[31] M. Klindworth, A. Piel, A. Melzer, U. Konopka, H. Rothermel, K. Tarantik, and G. E. Morfill, Phys. Rev. Lett. **93**, 195002 (2004).
[32] J. Goree, G. E. Morfill, V. N. Tsytovich, and S. V. Vladimirov, Phys. Rev. E **59**, 7055 (1999).
[33] M. R. Akdim and W. J. Goedheer, Phys. Rev. E **65**, 015401(R) (2001).
[34] S. L. Ossakow, K. Papadopoulos, J. Orens, and T. Coffey, J. Geophys. Res. **80**, 141 (1975).
[35] K. Miyamoto, *Plasma Physics for Nuclear Fusion*, revised ed. (MIT Press, Cambridge, MA, 1989).
[36] B. D. Fried and S. D. Conte, *The Plasma Dispersion Function* (Interscience, New York, 1961).
[37] K. Rönnmark (unpublished).
[38] A. Tjulin, A. Eriksson, and M. André, J. Plasma Phys. **64**, 287 (2000).
[39] L. S. Frost, Phys. Rev. **105**, 354 (1957).
[40] S. A. Khrapak, A. Ivlev, S. K. Zhdanov, and G. E. Morfill, Phys. Plasmas **12**, 042308 (2005).
[41] A. P. Nefedov *et al.*, New J. Phys. **5**, 33.1 (2003).
[42] A. V. Ivlev, H. M. Thomas, G. E. Morfill, V. I. Molotkov, A. M. Lipaev, V. E. Fortov, T. Hagl, H. Rothermel, and S. Krikalev, New J. Phys. **8**, 25 (2006).
[43] G. Joyce, M. Lampe, and G. Ganguli, Phys. Rev. Lett. **88**, 095006 (2002).
[44] V. Land and W. J. Goedheer, New J. Phys. **8**, 8 (2006).